ChemComm

Accepted Manuscript

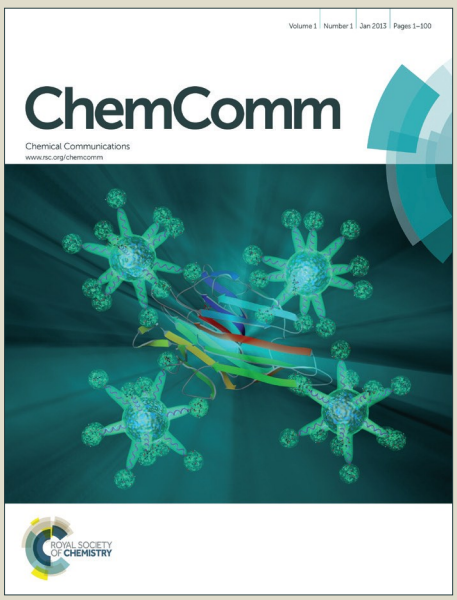

ROYAL SOCIETY OF CHEMISTRY

www.rsc.org/chemcomm

ChemComm

COMMUNICATION

Shape-controlled synthesis of $Cu_{31}S_{16}$-metal sulfide heteronanostructures *via* a two-phase approach

Received 00th January 20xx,
Accepted 00th January 20xx

DOI: 10.1039/x0xx00000x

www.rsc.org/

Miao Wang,[a] Aiwei Tang,*[ab] Lan Peng,[ab] Chunhe Yang[a] and Feng Teng*[b]

A series of different-shaped $Cu_{31}S_{16}$-metal sulfide (ZnS, CdS and $CuInS_2$) heteronanostructures have been synthesized by using a simple two-phase approach for the first time. This two-phase approach may shed light on the synthesis of $Cu_{31}S_{16}$-based heteronanostructures.

Semiconductor heteronanostructures (HNS), often consisting of two or more different types of materials with diverse functionalities, have attracted increasing interests over the past tens of years due to their integrated capabilities of the components.[1-3] To date, different types of HNS have been exploited, including metal-metal(Au-Ag, $CoPt_3$-Au),[4] semiconductor-semiconductor (CdSe-CdS, Cu_2S-PbS),[5] metal-semiconductor (Au-PbS, CdS-Au),[6] magnetic-semiconductor (CdS-Fe_3O_4, MnS-$Cu_{1.94}S$),[7] which combine the optical, electrical and magnetic properties of disparate components. These multifunctional properties will undoubtedly bring about new applications in optoelectronic devices, biological sensing,[5] energy conversion and so on.[3] Therefore, enormous efforts have been devoted to exploring different strategies for synthesizing the HNS materials, in which the wet-chemistry approach is one of the most popular synthetic methods.[8] In the wet-chemistry syntheses, HNS with special properties can be obtained by guiding the crystal growth along specific directions through the choice of the coordinating solvents and stabilizing agents. With the development of the wet-chemistry synthetic methods, two typical colloidal routes have been received a great deal of attention: seeded growth and catalyst-assisted growth.[2a, 5b].

Since Han et al firstly demonstrated $Cu_{1.94}S$ nanocrystals could serve as the catalyst for synthesis of one-dimensional Cu_2S-In_2S_3 HNS with different morphologies, research on the synthesis and applications of HNS has expanded tremendously in the past few years.[8, 9] The growth mechanism of HNS is believed to arise from the intrinsic cationic deficiencies and high cationic mobility of $Cu_{1.94}S$ nanocrystals. It is generally accepted that the Cu atoms in $Cu_{1.94}S$ behave like a "fluid" under relatively high temperature, which gives birth to another nanocrystal through the cation exchange process.[9] As a result, a variety of colloidal routes has been developed for preparing $Cu_{1.94}S$-based HNS, including hot-injection strategy,[2a, 8] one-pot colloidal approach as well as the single-precursor decomposition method.[9] As far as we know, however, there is no report on the synthesis of $Cu_{1.94}S$-based HNS via a simple two-phase approach.

The two-phase synthetic method is a powerful strategy for preparing different inorganic nanocrystals due to its low cost and environmental benignity.[10] Very recently, our group reported controllable synthesis of metal sulfide nanocrystals via such a two-phase approach, in which the nucleation and growth process took place at the water/oil interface.[11] Herein, this simple two-phase approach has been extended to prepare a series of $Cu_{31}S_{16}$-metal sulfide (ZnS, CdS and $CuInS_2$) HNS for the first time. The morphology of the $Cu_{31}S_{16}$-ZnS HNS can be tailored by varying the molar ratios of Cu/Zn precursors and the reactivity of Zn precursors. What's more, waterdrop-shaped $Cu_{31}S_{16}$-CdS and matchstike-like $Cu_{1.94}S$-$CuInS_2$ HNS have also been successfully synthesized. This two-phase strategy may shed light on synthesis of semiconductor HNS.

In a typical synthesis of icecream-like $Cu_{31}S_{16}$-ZnS HNS, $Cu(NO_3)_2$ (0.5 mmol) and $Zn(NO_3)_2$ (1.0 mmol) were added into 20 mL of deionized water under magnetic stirring, and then transferred into a 50 mL Teflon-lined autoclave. Afterwards, 1-dodecanethiol (DDT, 3 mL) was added into the aqueous solution to form a two-phase solution. In this two-phase reaction system, DDT was the upper oil phase, which acted as not only a sulfur source, but also a surface-capping agent and reducer. The lower aqueous phase was consisted of metal salts solution. Finally, the Teflon-lined autoclave was sealed and then kept at 190 °C for 20 h. Different-shaped $Cu_{31}S_{16}$-ZnS HNS were synthesized using the same process except the Cu/Zn precursor ratios. The experimental details are given in ESI†. As shown in Fig.1a and b, the transmission electron microscopy (TEM)

[a] *Department of Chemistry, School of Science, Beijing JiaoTong University, Beijing 100044, PR China. E-mail: awtang@bjtu.edu.cn; Tel: +86 10 51683627*
[b] *Key Laboratory of Luminescence and Optical Information, Ministry of Education, Beijing JiaoTong University, Beijing 100044, PR China. E-mail: fteng@bjtu.edu.cn*
†*Electronic Supplementary Information (ESI) available:* HRTEM image and XPS spectra of icecream-like $Cu_{31}S_{16}$-ZnS HNS, XRD patterns and TEM images of $Cu_{31}S_{16}$-ZnS HNS synthesized using different Zn sources for different reaction time, TEM images and HRTEM images of $Cu_{31}S_{16}$-CdS HNS synthesized by using the molar ratios of Cu/Cd precursors of 2:1, XRD patterns, TEM images and optical spectra of CdS:Cu nanocrystals as well as the TEM images and EDX results of $Cu_{31}S_{16}$-$CuInS_2$ HNS synthesized by using Cu/In precursor ratio of 1:1. *See DOI: 10.1039/x0xx00000x*

images reveal that the products exhibit a short matchstick- and mushroom-like shape when the molar ratios of $Cu(NO_3)_2/Zn(NO_3)_2$ are 2:1 and 1:1. As the molar ratio of Cu/Zn precursor is further decreased to 1:2, uniform icecream-like $Cu_{31}S_{16}$-ZnS HNS can be obtained (Fig.1c). To the best of our knowledge, the icecream-like HNS are reported for the first time. High-resolution TEM (HRTEM) images were employed to study the detailed structure and boundary information of the icecream-like HNS. As shown in Fig.1d and Fig.S1a†, an obvious boundary is observed between the two materials in a single icecream nanocrystal (boundary highlighted by the white line). The distance between the adjacent lattice fringe of the head is measured to be 0.337 nm, which can be indexed as the (004) plane of $Cu_{31}S_{16}$.The lattice spacing of 0.311 nm in the stem corresponds to (002) plane of ZnS (Fig.1d). The HRTEM result reveals that the (004) plane of $Cu_{31}S_{16}$ coincides with the (002) plane of ZnS. The corresponding fast Fourier transformation (FFT) patterns shown in Fig.S1b and c† obtained from the head and stem of the icecream-like HNS confirm the presence of two distinct phases in the product and single-crystalline nature of the nanocrystals. X-ray photoelectron spectra (XPS) were employed to characterize the composition and valence state of the icecream-like $Cu_{31}S_{16}$-ZnS HNS (Fig.S2†), which demonstrates the different chemical environment of the formation of Cu-S and Zn-S bonds.

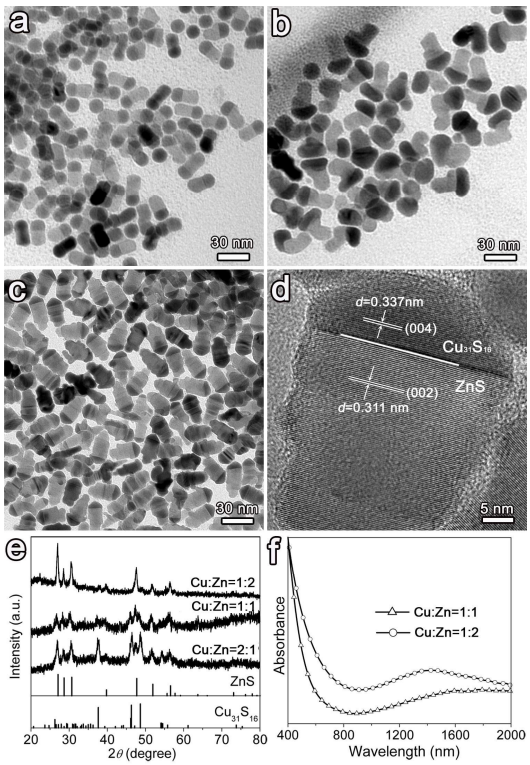

Fig.1 TEM images of different-shaped $Cu_{31}S_{16}$-ZnS HNS: (a) short matchstick (Cu:Zn=2:1); (b) mushroom(Cu:Zn=1:1) (c) icecream(Cu:Zn=1:2); (d) HRTEM image of a single icecream-like particle shown in Fig.1(c); (e) XRD patterns of different-shaped $Cu_{31}S_{16}$-ZnS HNS, and the bottom lines represent the standard diffraction peaks of monoclinic $Cu_{31}S_{16}$ (JCPDS No.23-0959) and wurtzite ZnS (JCPDS No.36-1450); (f) Vis-NIR absorption spectra of $Cu_{31}S_{16}$-ZnS HNS synthesized by using different molar ratios of Cu/Zn sources .

The X-ray diffraction (XRD) patterns of different-shaped $Cu_{31}S_{16}$-ZnS HNS are given in Fig.1e As shown in Fig.1e that the as-obtained different-shaped HNS are composed of monoclinic $Cu_{31}S_{16}$ (JCPDS No.23-0959) and wurtzite ZnS (JCPDS No.36-1450). It should be noted that the diffraction peaks assigned to wurtzite ZnS become stronger in intensity but the intensity of three main peaks belonging to monoclinic $Cu_{31}S_{16}$ phase gets weaker with the decrease of the molar ratio of Cu/Zn sources from 2:1 to 1:2. The diffraction peaks of wurtzite ZnS phase are almost dominant over the icecream-like HNS, which indicates that the morphology and crystal phase were very sensitive to the concentration of the metal ions.

The optical absorption spectra of mushroom-like and icecream-like $Cu_{31}S_{16}$-ZnS HNS show a broad near-infrared (NIR) absorbance between 800-2000 nm (Fig.1f). On the basis previous results, the NIR absorbance observed in the spectra originates from the localized surface plasmon resonance (LSPR) of the copper sulfide with deficient copper due to excess holes in the valence band. [12]A blue-shift of LSPR peak is observed in the icecream-like HNS as compared to that of mushroom-like HNS. Accordingly, the density of free holes is increased from 5.1×10^{21} to 5.5×10^{21} cm^{-3} based on the Mie-Drude model (Fig. S3†).The increase of the density of free holes can be explained as follows: more ZnS epitaxially attaches to $Cu_{31}S_{16}$ which makes the electric field intensify, resulting in an increase of free holes in the $Cu_{31}S_{16}$ stem.[12a]

To gain understanding the formation mechanism of the $Cu_{31}S_{16}$-ZnS HNS synthesized by this two-phase approach, we performed a series of experiments involving the syntheses of short matchstick-like and icecream-like $Cu_{31}S_{16}$-ZnS HNS for different reaction time. When the molar ratio of Cu/Zn precursors is kept 2:1, the main phase of the product obtained at 5 h is monoclinic $Cu_{31}S_{16}$ and then the wurtzite ZnS appears, and the diffraction intensity of the ZnS phase becomes stronger with the reaction time increasing (Fig.S4†). Considering that the complexity of the $Cu_{2-x}S$ NCs, the comparison of the diffraction peaks between the as-obtained product and four different bulk $Cu_{2-x}S$ phases is given in Fig.S5†. When the molar ratio of Cu/Zn precursors is decreased to 1:2, a very different experimental phenomenon is observed that hexagonal ZnO phase appears in the intermediate stage of the reaction which is then used up during the further reaction (Fig.S6†). Based on the aforementioned results, a plausible formation mechanism of $Cu_{31}S_{16}$-ZnS HNS is proposed. Firstly, the metal ions can migrate to the water/oil interface to react with DDT to form monolayer-capped metal clusters through the S atoms on the basis of our previous report.[11] In this reaction system, the mobility of the Cu and Zn ions is comparative, and they can reach the water/oil interface at about the same time. It is well known that the Cu ions have stronger coordination abilities with DDT than Zn ions, thus the monoclinic $Cu_{31}S_{16}$ nuclei can be firstly formed which can serve as the seeds for further growth. In the case of lower Cu/Zn molar ratio, the Zn ions at the interface can react with DDT to generate ZnS monomer which is formed at one side of $Cu_{31}S_{16}$, thus the matchstick-like HNS are obtained. In contrast, massive Zn^{2+} can reach the interface and the amount of DDT is not enough in the case of higher Cu/Zn molar ratio, and the superfluous Zn^{2+} can react with oxygen to promote the formation of ZnO phase. With the epitaxial growth of ZnS onto one side of $Cu_{31}S_{16}$, more Cu ions are

repelled out of the lattice and Zn ions occupy their vacant sites, finally the ZnO can be used out during the further reaction. As a result, the morphology evolves from short matchstick to mushroom and the icecream-like HNS are finally obtained with the molar ratios of Cu/Zn precursors decreasing.

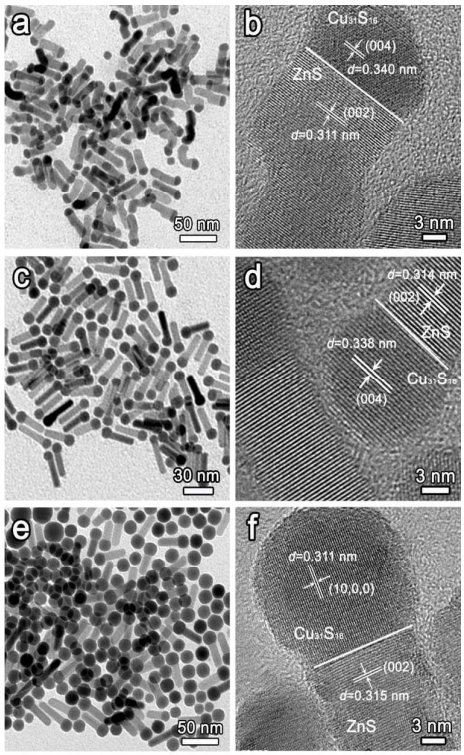

Fig. 2 TEM (left) and HRTEM (right) images of different-shaped $Cu_{31}S_{16}$-ZnS HNS synthesized by using different Zn sources:(a, b) $Zn(OAc)_2$; (c,d)$ZnSO_4$; (e,f) $ZnCl_2$.

To further verify the formation mechanism of the $Cu_{31}S_{16}$-ZnS HNS, different Zn sources including $Zn(OAc)_2$, $ZnSO_4$ and $ZnCl_2$ were used in the synthesis of HNS while the molar ratio of Cu/Zn sources was kept at 1:2. Fig.2 depicts the low-magnification TEM and HRTEM images of $Cu_{31}S_{16}$-ZnS HNS by using different Zn sources. As shown in Fig.2a, matchstick- and tadpole-like HNS are obtained in the HNS synthesized by using $Zn(OAc)_2$ as Zn source. A clear boundary between the two different materials is observed in the HRTEM images (Fig.2b), and the lattice fringes can be indexed as (004) planes of $Cu_{31}S_{16}$ and (002) of ZnS, suggesting that the growth of ZnS stem is along the <001> direction. When $ZnSO_4$ was used as Zn source, uniform matchstick-like HNS were obtained (Fig.2c), and the average diameter of $Cu_{31}S_{16}$ head is 10.8±0.8 nm, the average length and width of ZnS stick are 24.1±3.2 and 7.0±0.7 nm, respectively. An interplanar distance analysis of the HRTEM image shown in Fig.2d reveals that the ZnS stick epitaxially attaches to the (004) planes of $Cu_{31}S_{16}$ head through its (002) plane. If the Zn source is changed to $ZnCl_2$, matchstick-like $Cu_{31}S_{16}$-ZnS HNS and isolated spherical $Cu_{31}S_{16}$ nanocrystals will coexist in the as-synthesized samples (Fig.2e), and the average diameter of $Cu_{31}S_{16}$ head is 16.7±2.5 nm, which is very close to that of isolated $Cu_{31}S_{16}$ nanocrystals (16.1±1.9 nm). The corresponding HRTEM image shown in Fig.2f also confirms that the ZnS stem grows along its <001> direction on the {100} facets of $Cu_{31}S_{16}$ head. The XRD patterns of the products synthesized by using three different Zn sources indicate that they are composed of monoclinic $Cu_{31}S_{16}$ and wurtzite ZnS phase (Fig.S7†). It should be pointed out that the diffraction peaks from $Cu_{31}S_{16}$ phase are dominant over the XRD patterns of the sample synthesized by using $ZnCl_2$ as Zn sources due to the presence of isolated $Cu_{31}S_{16}$ nanocrystals (Fig.S7c†). Based on the above experimental results, it can be concluded that the different anions in the Zn sources lead to the variation of the morphology and crystal structure of the three samples. In the two-phase syntheses, the drift speed of the metal ions to the water/oil interface is of great importance for the nucleation and growth, while the reaction rate can be adjusted in the presence of different anions. It is stated previously that Cl^- is a strong ligand which can bond with some Cu ions to form $CuCl_4^{2-}$, causing a slower drift speed.[10b] As a consequence, once the $Cu_{31}S_{16}$ nuclei are formed, the ZnS grows epitaxially along the boundary direction subsequently. With the exhaustion of Zn ions, the $CuCl_4^{2-}$ ions reach the interface and self-nucleate to form isolated $Cu_{31}S_{16}$ nanocrystals. In contrast, the OAc^- is a weak ligand, which can slow the reaction, but the self-nucleation doesn't take place. The growth rate is slower in the presence of SO_4^{2-} than that of NO_3^- due to the relative stronger electrostatic interaction, thus the matchstick HNS are obtained instead of icecream-like HNS when $ZnSO_4$ is used as Zn sources. More interestingly, the matchstick-like HNS can self-assemble into head to tail arrangements (Fig.S8†), which is also observed in previous work, and they attributed the self-assembly behavior to the electric dipole-dipole interactions.[8a]

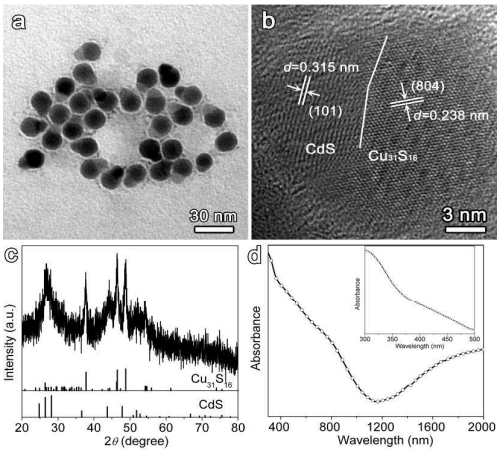

Fig. 3 (a)TEM and (b) HRTEM Images of $Cu_{31}S_{16}$-CdS HNS synthesized Cu/Cd ratio being 2:1; (c) the corresponding XRD patterns, the bottom lines represent the standard diffraction peaks of monoclinic $Cu_{31}S_{16}$ (JCPDS No.23-0959) and wurtzite CdS (JCPDS No.41-1049) ; (d) absorption spectra, and the inset shows the absorption spectra in the region from 300 to 500 nm.

Considering that the Zn and Cd belong to the same group, it is predicted that this two-phase approach can be extended to prepare $Cu_{31}S_{16}$-CdS HNS. As shown in Fig.3a, the as-synthesized sample exhibits a waterdrop-like shape when the molar ratio of Cu/Cd is kept 2:1. The corresponding HRTEM analysis shown in Fig.3b demonstrates the coexistence of the two different materials by a

clear boundary, and the distance of adjacent lattice fringes of one part is 0.315 nm, which can be indexed as the (101) planes of wurtzite CdS phase. In contrast, the lattice spacing of the other part is 0.238 nm, which can be assigned to the (804) plane of monoclinic $Cu_{31}S_{16}$. Further evidence of the formation of $Cu_{31}S_{16}$-CdS HNS is confirmed by the XRD patterns shown in Fig.3c, and all the diffraction peaks match well with the monoclinic $Cu_{31}S_{16}$ and wurtzite CdS (JCPDS No.41-1049). Apart from the waterdrop-like HNS, some isolated $Cu_{31}S_{16}$ nanocrystals and ellipsoid HNS are also obtained (Fig.S9a†), which can be verified by the HRTEM images (Fig.S9b and c†). A weak but broad absorption band in the region of 300-1200 nm is observed, which may evoke by the transition from Cu doping level to the valence band of CdS as well as the direct transition in $Cu_{31}S_{16}$.[13] Moreover, a NIR absorption peak beyond 1200 nm appears in the optical absorption spectrum (Fig.3d), which is derived from LSPR band from Cu-deficient $Cu_{31}S_{16}$. The radius of Cd atoms is larger than that of Cu atoms, which makes the mobility of Cd ions lower than that of Cu ions, thus the Cu ions can reach the interface earlier than Cd ions. As aforementioned that $Cu_{31}S_{16}$ particle is firstly generated at the interface, and then CdS can epitaxially grow onto the boundary of $Cu_{31}S_{16}$. It is difficult for cation exchange of Cd ions due to the higher energy barrier resulting from the different atoms size. Therefore, the CdS takes up smaller volume of HNS. With an increase in Cd precursors, the highly fluidic nature of the Cu ions enables the saturated Cd ions to self-nucleate to form CdS phase, followed by the doping of Cu ions into the CdS host. As a control experiment, further decreasing the molar ratio of Cu/Cd precursors to 2:3 leads to the formation of cubic CdS:Cu(I) phase (Fig.S10a†). Additionally, uniform CdS:Cu (I) nanospheres are dominant over the as-obtained products, and their average size is less than 5 nm (Fig.S10b†). No NIR absorbance is observed in the Vis-NIR absorption spectrum (Fig.S11a†), but an absorption peak at around 395 nm is observed (Fig.S11b†). Moreover, a PL maximum at 626 nm with a shoulder at 673 nm is detected, which originates from the dopant emission and the surface-trap emission.[13a]

What's more, to extend this two-phase strategy to prepare more types of $Cu_{31}S_{16}$-based HNS, short matchstick-like $Cu_{31}S_{16}$-$CuInS_2$ HNS were successfully synthesized by this two-phase approach (Fig.S12a†). The HRTEM image (Fig.S12b†) and XRD patterns (Fig.S12c†) indicate that the HNS are composed of monoclinic $Cu_{1.94}S$ and wurtzite $CuInS_2$ phases, which is further confirmed by the line-scan energy-dispersive X-ray spectroscopy (Fig.S13†). The elemental profiles demonstrate that Cu and S elements spread throughout the whole HNS, and the In element is limited in to the stick part. As a matter of fact, the $Cu_{1.94}S$-$CuInS_2$ HNS have been synthesized by other colloidal approaches, which is an essential intermediate step in the growth of ternary $CuInS_2$ nanocrystals.[8b,c,9d] The study on the synthesis of ternary I-III-V_2 nanocrystals by this two-phase approach is going on.

In summary, different-shaped $Cu_{31}S_{16}$-metal sulfide (ZnS, CdS and $CuInS_2$) HNS have been synthesized by using a simple two-phase approach for the first time. The shape and crystal structures of $Cu_{31}S_{16}$-ZnS HNS can be effectively tailored by varying the molar ratios of Cu/Zn precursors and anions in Zn sources. This two-phase approach may provide a general method to prepare $Cu_{31}S_{16}$-based HNS with unique or multifunctional properties for widely application in optoelectronic devices and catalytic fields.

This work is partly supported by the Fundamental Research Funds for the Central Universities (2014JBZ010), and National Natural Science Foundation for Distinguished Young Scholars of China (61125505). The authors (M.W) appreciate the support from the Fundamental Research Funds for the Central Universities (S15JB00380).

Notes and references

1 (a) D.V. Talapin, J.-S. Lee, M.V. Kovalenko and E.V. Shevchenko, *Chem. Rev.,* 2010, **110**, 389-458. (b) L. Carbonea and P. D. Cozzolia, *Nano Today.,* 2010, **5**, 449-493. (c) J. Kolny-Olesiak. *CrystEngComm.,* 2014, 16, 9381-9390.

2 (a) W. Han, L. Yi, N. Zhao, A. Tang, M. Gao and Z. Tang, *J. Am. Chem. Soc.*, 2008, **130**, 13152-13161.(b) P. D.Cozzoli, T. Pellegrino and L. Manna, *Chem. Soc. Rev.* , 2006, **35**, 1195-1208.

3 (a) O. Hayden, R. Agarwal and C. M. Lieber, *Nat. Mater.,* 2006, **5**, 352–356. (b) A. W. Tang, F. Teng, Y. Wang, Y. B. Hou, W. Han, L. X. Yi and M. Y. Gao, *Nanoscale. Res. Lett.,* 2008, **3**, 502-507. (c) J. Choi, Y. Jun, S. Yeon, H. C. Kim, J-S. Shin and J. Cheon, *J. Am. Chem. Soc.,* 2006, **128**, 15982-15983. (d) Y. X. Li, G. Chen, C. Zhou and J. X. Sun, *Chem.Comm*., 2009, 2020-2022. 4 (a) T. Pellegrino, A. Fiore, E. Carlino, C. Giannini, P. D. Cozzoli, G. Ciccarella, M. Respaud, L. Palmirotta, R. Cingolani and L. Manna, *J. Am. Chem. Soc*., 2006, **128**, 6690-6698. (b) X. Hong, D. S. Wang, R. Yu, H. Yan, Y. Sun, L. He, Z. Q. Niu, Q. Peng and Y. D. Li, *Chem. Comm*., 2011, **47**, 5160-5162.

5 (a) L. Ouyang, K. N. Maher, C. L. Yu, J. McCarty and H. K. Park, *J. Am. Chem. Soc.,* 2007, **129**, 133-138. (b) T. T. Zhuang, F. J. Fan, M. Gong and S. H. Yu, *Chem. Comm.,* 2012, **48**, 9762-9764.(c) D. V. Talapin, J. H. Nelson, E. V. Shevchenko, S. Aloni, B. Sadtler and A. P. Alivisatos, *Nano Lett*., 2007, **7**, 2951-2959.

6 (a) W. Shi, H. Zeng, Y. Sahoo, T. Y. Ohulchanskyy, Y. Ding, Z. L. Wang, M. Swihart and P. N. Prasad, *Nano Lett.*, 2006, **6**, 875-881. (b)A. E. Saunders, I. Popov, U. Banin, *J. Phys. Chem. B.,* 2006, **110**, 25421-25429.

7(a) K. W. Kwon, B. H. Lee and M. Shim, *Chem. Mater.*, 2006, **18**, 6357-6363. (b) J. C. Zhou, F. Huang, J. Xu and Y. S. Wang, *CrystEngComm.*, 2013, **15**, 4217-4220.

8. (a)L. Yi, A. Tang, M. Niu, W. Han, Y. Hou and M. Gao, *CrystEngComm*, 2010, **12**, 4124-4130. (b) J. Li, M. Bloemen, J. Parisi and J. Kolny-Olesiak, *ACS Appl. Mater. Interfaces*., 2014, 6, 20535-20543. (c) M. Kruszynska, H. Borchert, J. Parisi and J. Kolny-Olesiak, *J. Am. Chem. Soc.* 2010, 132, 15976-15986.

9. (a) H. Ye, A. Tang, L. Huang, Y. Wang, C. Yang, Y. Hou, H. Peng, F. Zhang and F. Teng, *Langmuir*, 2013, **29**, 8728-8735.(b) J-Y.Chang, C-Y. Cheng. *Chem. Comm*., 2011, **47**, 9089-9091.(c) S. K. Han, M. Gong, H. B. Yao, Z. M. Wang and S. H. Yu, *Angew. Chem. Int. Ed.*, 2012, **51**, 6365-6368. (d) S. T. Connor, C-M. Hsu, B. D. Weil, S. Aloni and Y. Cui, J. Am. Chem. Soc., 2009, 131, 4962-4966.

10. (a) L. Hu, M. Chen, X. Fang and L. Wu, *Chem. Soc. Rev.*, 2012, **41**, 1350–1362. (b) Z. Zhuang, Q. Peng, B. Zhang and Y. Li, *J. Am. Chem. Soc.*, 2008, **130**, 10482–10483.

11. M. Wang, A. W. Tang, D. X. Zhu, C. H. Yang and F. Teng, *CrystEngComm.*, 2015, **17,** 6598-6606.

12. (a) H. Ye, A. Tang, Y. Hou, C. Yang and F. Teng, *Opt. Mater. Express.,* 2014, **4**, 220-226. (b) H. Ye, A. Tang, C. Yang, K. Li, Y. Hou and F. Teng, *CrystEngComm*., 2014, **16**, 8684-8690. (c) Y. Xie, L. Carbone, C. Nobile, V. Grillo, S. D'Agostino, F. D. Sala, C. Giannini, D. Altamura, C. Oelsner, C. Kryschi and P. D. Cozzoli, *ACS Nano*., 2013, 7, 7352-7369. (d) A. Comin and L. Manna, *Chem. Soc. Rev.* , 2014, 43, 3957-3975.

13. (a) A. W. Tang, L. X. Yi, W. Han, F. Teng, Y. S. Wang, Y. B. Hou and M. Y. Gao. *Appl. Phys. Lett.,* 2010, **97**, 033112. (b) I. Kriegel, J. Rodríguez-Fernández, E. Dacomo, A. A. Lutich, J. M. Szeifert, and J. Feldmann, *Chem. Mater.*, 2011, **23**, 1830–1834.

